COMMUNICATIONS PHYSICS

ARTICLE

DOI: 10.1038/s42005-018-0089-1 OPEN

Control of tunneling in an atomtronic switching device

Karin Wittmann Wilsmann[1], Leandro H. Ymai[2], Arlei Prestes Tonel[2], Jon Links[3] & Angela Foerster[1]

The precise control of quantum systems will play a major role in the realization of atomtronic devices. As in the case of electronic systems, a desirable property is the ability to implement switching. Here we show how to implement switching in a model of dipolar bosons confined to three coupled wells. The model describes interactions between bosons, tunneling of bosons between adjacent wells, and the effect of an external field. We conduct a study of the quantum dynamics of the system to probe the conditions under which switching behavior can occur. The analysis considers both integrable and non-integrable regimes within the model. Through variation of the external field, we demonstrate how the system can be controlled between various "switched-on" and "switched-off" configurations.

[1] Instituto de Física da UFRGS, Av. Bento Gonçalves 9500, Agronomia, Porto Alegre 91501-970 RS, Brazil. [2] Universidade Federal do Pampa, Av. Maria Anunciação Gomes de Godoy 1650, Bairro Malafaia, Bagé 96413-170 RS, Brazil. [3] School of Mathematics and Physics, The University of Queensland, Brisbane, QLD 4072, Australia. Correspondence and requests for materials should be addressed to J.L. (email: jrl@maths.uq.edu.au)

The phenomenon of quantum tunneling is paramount in many studies of ultracold quantum gases. The two-well Bose–Hubbard Hamiltonian has been very successful in modeling quantum tunneling[1,2], displaying two principal dynamical scenarios. These are referred to as Josephson tunneling and self-trapping, and they have been experimentally observed[3]. In the case of tunneling, the system can also be controlled to produce either alternating or direct currents[4]. A three-well system opens up wider possibilities for physical behaviors[5–7], most notably as an ultracold version of a transistor[8], or similar type of switching device. The individual wells can be identified as the source, gate, and drain, potentially forming a building block in the emerging field of atomtronics[9–11]. This prospect is driving research into transistor-like structures beyond the electronic domain[12,13].

Here we investigate the influence of integrability in the control of tunneling in a triple-well system. To do so, we must go beyond the familiar three-well Bose–Hubbard model[14–18], and consider a more general system which facilitates an integrable limit. Such a model has already been introduced into the literature. It models dipole–dipole interactions and the tunneling between adjacent sites for a population of ultracold dipolar bosons with large dipole moment, such as chromium or dysprosium, loaded in an aligned triple-well potential. The Hamiltonian has the general structure[19]

$$\begin{aligned}\mathcal{H} =& \frac{U_0}{2}\sum_{i=1}^{3} N_i(N_i-1) + \sum_{i=1}^{3}\sum_{j=1;j\neq i}^{3}\frac{U_{ij}}{2}N_iN_j \\ & - J_1(a_1^\dagger a_2 + a_1 a_2^\dagger) - J_3(a_2^\dagger a_3 + a_2 a_3^\dagger).\end{aligned} \tag{1}$$

The canonical creation and annihilation operators, $a_i^\dagger$ and a_i, $i=1,2,3$, represent the three bosonic degrees of freedom in the model, and $N_i = a_i^\dagger a_i$, $i=1,2,3$ is the number operator for each well. The parameters J_i, $i=1,3$ are the couplings for the tunneling between wells, and U_0 is the coupling constant for on-site interactions which results from contact interactions and dipole–dipole interactions (DDI). Both of these can be either attractive or repulsive, which in principle allows for the manufacture of weak net on-site interaction. The parameters $U_{ij}=U_{ji}$, $i\neq j$ characterize DDI between particles on different sites. Although the DDI follows an inverse cubic law, it is also dependent on the angle between dipole orientation and the displacement between dipoles. In combination with the geometry of the trap potential (viz. oblate versus prolate), it is entirely feasible to adjust the system parameters across a wide range of values. Importantly, this includes the possibility for the inter-well couplings U_{ij} to have greater magnitude than the on-site coupling U_0. The experimental feasibility of this system for dipolar bosons was detailed by Lahaye et al.[19], using a triple-well potential. The wells are aligned along the y-axis, separated by a distance l, with bosons polarized by a sufficiently large external field along the z-direction. It was shown that $U_{12}=U_{23}=\alpha U_{13}$, where the parameter $4\leq\alpha\leq 8$ depends only on the ratio l/σ_x, where σ_x is the width of the Gaussian cloud along the x-direction. (See Methods for further details.)

In the case when $U_{13}=U_0$, the Hamiltonian (1) is integrable[20]. In this limit there exists an additional conserved operator besides the Hamiltonian and the total particle number, such that the number of independent conserved operators is equal to the number of degrees of freedom. While for classical systems integrability is well-known to prohibit chaotic behavior, the consequences for quantum system are less understood[21,22]. Notwithstanding, it is recognized that quantum integrability has far reaching impacts. One route to characterize the degree of chaoticity in a quantum system is through energy level spacing distributions[23]. Integrable systems tend to display Poissonian distributions[24], while non-integrable systems generally observe the Wigner surmise[25] following the Gaussian Orthogonal Ensemble, or similar[26,27]. Another impact of quantum integrability is the absence of thermalization, observed in a quantum version of Newton's cradle[28] and similar systems[29]. Here we demonstrate how integrability, and the breaking of it, can be utilized to investigate tunneling dynamics. This work contrasts the above mentioned studies in that it applies to a system with very low number of degrees of freedom.

A simple means of breaking integrability in the model is through an applied external field. Generally, it might be expected that this will drive the system into a chaotic dynamical regime. However it is shown that in certain circumstances the changing dynamics of the model, through tuning of the external field, can be predicted with remarkable accuracy. The result can be understood by revealing the structure of a hidden subsystem within the model. This level of control points towards the potential utility of a physical realization of the model as a quantum switch.

Results

Integrability. It has been established that the model (1) contains a family of integrable three-well tunneling models when $U_{13}=U_0$[20]. In this case, we can write the Hamiltonian in the reduced form $H_0 = -\mathcal{H} + (\alpha+1)U_0N^2/4 - U_0N/2$ yielding

$$\begin{aligned}H_0 =& U(N_1-N_2+N_3)^2 \\ & + J_1(a_1^\dagger a_2 + a_1 a_2^\dagger) + J_3(a_2^\dagger a_3 + a_2 a_3^\dagger),\end{aligned} \tag{2}$$

where $U=(\alpha-1)U_0/4$. Note that (2) commutes with the total number operator $N=N_1+N_2+N_3$, and the interchange of the indices 1 and 3 leaves the Hamiltonian invariant. The Hamiltonian has, beyond the energy and the total number of particles N, another independent conserved quantity expressed through the operator[20]

$$Q = J_1^2N_3 + J_3^2N_1 - J_1J_3(a_1^\dagger a_3 + a_3^\dagger a_1). \tag{3}$$

This conserved operator can alternatively be interpreted as a tunneling Hamiltonian for a two-well subsystem containing only wells 1 and 3. Because Q admits the factorization $Q=\Omega^\dagger\Omega$, where $\Omega = J_1a_3 - J_3a_1$, the dynamical evolution governed by Q is harmonic for any initial state. Later, it will be shown that Q assumes a fundamental role in the analysis of resonant[30] quantum dynamics of the system (2). This arises due to an unexpected connection with virtual processes. Details are provided in Methods.

As the model has three degrees of freedom and three independent conserved quantities satisfying

$$[H_0,N]=0, \quad [H_0,Q]=0, \quad [N,Q]=0, \tag{4}$$

the model is integrable. Further details about the integrability, and associated exact solvability, have been established. This was achieved through the Yang-Baxter equation and Bethe Ansatz methods[20].

Breaking the integrability. In order to break the integrability, we add to the Hamiltonian (2) the operator $H_1=\varepsilon(N_3-N_1)$, which acts as an external field for the wells labeled 1 and 3. This is schematically shown in Fig. 1. It is important to observe that the above Hamiltonian still commutes with the operator N. However, the operator Q is not conserved because the commutator $[H,Q] = 2\varepsilon J_1J_3(a_1^\dagger a_3 - a_3^\dagger a_1)$ is non-zero when the parameters ε, J_1 and J_3 are all non-zero.

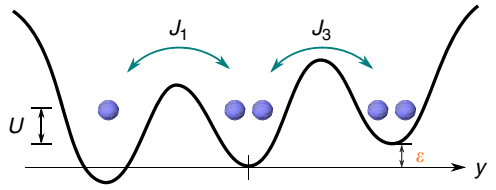

Fig. 1 Schematic representation of the system. With reference to the Hamiltonian $H = H_0 + H_1$, the arrows J_1 and J_3 represent the tunneling couplings between the wells, U characterizes inter-well and intra-well interaction between bosons, while ε is the coupling strength for an external field

Structure of energy levels. The integrable three-well system (2) possesses many features in common with the two-well Bose–Hubbard model, which is also integrable because the total number operator is conserved and there are only two degrees of freedom. Set $J = \sqrt{J_1^2 + J_3^2}$. Following Leggett[2], it is useful to define the regimes:

- Rabi: $U \ll JN^{-1}$.
- Josephson: $JN^{-1} \ll U \ll JN$.
- Fock: $JN \ll U$.

where in the two-well case the "Fock regime corresponds to a strongly quantum pendulum, while in the Rabi and Josephson regimes the behavior is (semi)classical"[2].

Adopting the same classification for the integrable three-well system given by (2), numerical computation of the energy spectrum shows that transition from the Rabi to the Josephson regime is accompanied by the emergence of energy bands. Illustrative results are depicted in Fig. 2. Hereafter units are chosen such that $\hbar = 1$, and for all figures isotropic tunneling $J_1/J = J_3/J = 1/\sqrt{2}$ is adopted for simplicity. The Hamiltonian acts on the Fock space spanned by the normalized vectors $|\mathcal{N}_1, \mathcal{N}_2, \mathcal{N}_3\rangle = \mathcal{C}^{-1}(a_1^\dagger)^{\mathcal{N}_1}(a_2^\dagger)^{\mathcal{N}_2}(a_3^\dagger)^{\mathcal{N}_3}|0\rangle$, where $\mathcal{C} = \sqrt{\mathcal{N}_1!\mathcal{N}_2!\mathcal{N}_3!}$ and $|0\rangle \equiv |0,0,0\rangle$ is the Fock vacuum. On each panel the line $E = UN^2$ is depicted. This quantity is the expectation value of the state $|N,0,0\rangle$. In the extreme Rabi regime with $U = 0$ the energy levels are uniformly distributed with spacing $\Delta E = J$. The line $E = UN^2$ emerges from the midpoint of the entire energy spectrum when $U = 0$, to lie on the lower edge of the uppermost energy band as U is increased to bring the system into the Josephson regime. Note that the separation into distinct energy bands becomes very evident once the system is deep into the Josephson regime. These features significantly influence the dynamical evolution of the system from the initial state $|N,0,0\rangle$. In the Rabi regime, an accurate description of the initial state requires a linear combination over all eigenstates. However in the Josephson regime the state $|N,0,0\rangle$ can be accurately approximated as a linear combination of a subset of eigenstates, due to the band structure. This conclusion applies for all particles numbers, with the result represented in Fig. 2 depicting the cases $N = 30$ and $N = 60$. Provided $UN/J \gg 1$, the separation into bands is clearly identifiable. The consequences will be investigated at a deeper level in the next section, where we will fix $N = 60$. Moreover, it will be shown how the breaking of the integrability, through the application of an external field, allows for control of the dynamics in a predictable fashion.

Quantum dynamics. The time evolution of the expectation values for the number operators are computed using $\langle N_i \rangle = \langle \Psi(t)|N_i|\Psi(t)\rangle$, $i = 1,2,3$, where $|\Psi(t)\rangle = \exp(-iHt)|\phi\rangle$ and $|\phi\rangle$ represents an initial state. We adopt a protocol for which

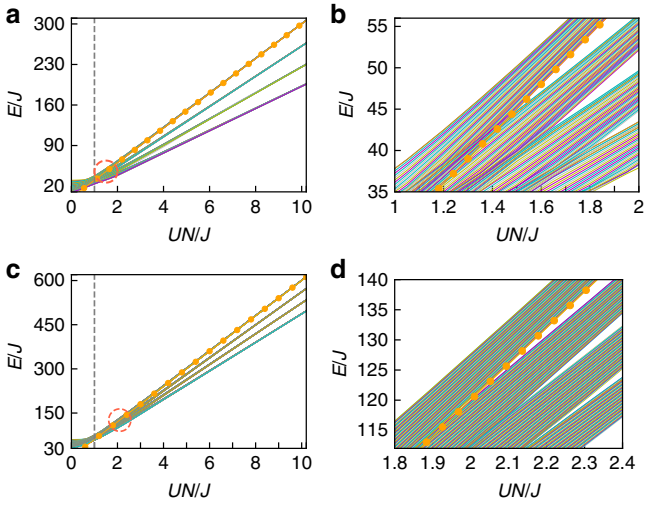

Fig. 2 Energy level distributions. Results are shown for (2) in dimensionless units. **a**, **b** $N = 30$. **c**, **d** $N = 60$. The region marked with a circle on **a** and **c** is enlarged in **b** and **d**. The dashed vertical lines mark the threshold point, $UN/J = 1$, separating Rabi and Josephson regimes. The ball lines mark the expectation energy $E = UN^2$ of $|N,0,0\rangle$. Only the four highest energy bands are plotted

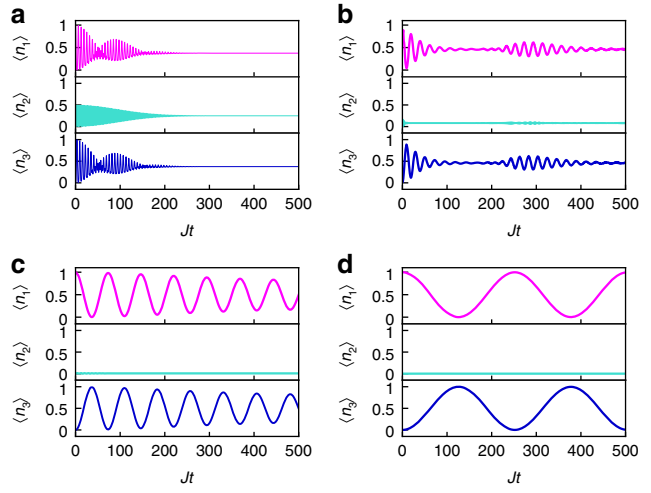

Fig. 3 Time evolution of expectation values. Dimensionless units are used. In the integrable regime, the expectation values of the number operators are shown, with the initial state $|60,0,0\rangle$. The configuration used has $\varepsilon/J = 0$. **a** $U/J = 0.001$; **b** $U/J = 0.015$; **c** $U/J = 0.05$; **d** $U/J = 0.17$. It is apparent that increasing U leads to an increasing suppression of tunneling into the gate, while maintaining oscillations between the source and the drain. In the case **d**, the expectation value of the number operator associated with the gate is negligible, so tunneling to the gate is considered to be switched-off. The oscillations between the source and the drain are close to being harmonic and coherent

$|\phi\rangle = |N,0,0\rangle$, so the well labeled 1 is the source, the well labeled 2 is the gate, and the well labeled 3 is the drain.

We begin with the integrable model (2) and first consider variations in the interaction parameter U to manipulate the tunneling across the wells. Figure 3 presents results obtained for four choices of U. The dynamics typically display collapse and revival of oscillations in the Rabi regime, as in Fig. 3a. On increasing U, the period increases while the time-average of $\langle N_2 \rangle$ decreases. Furthermore, the dynamics between wells 1 and 3

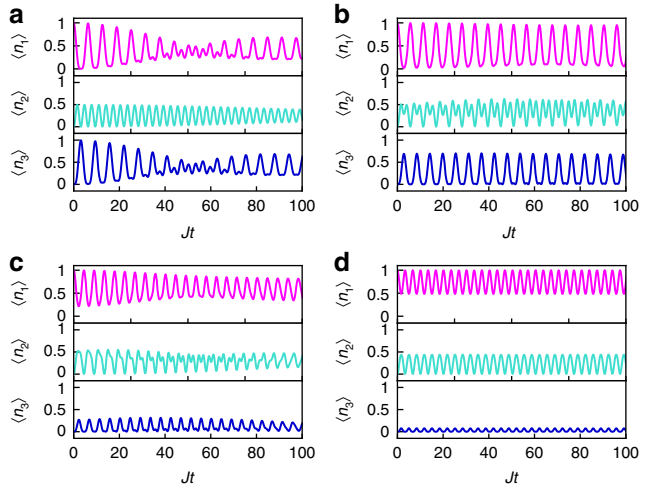

Fig. 4 Time evolution of expectation values. Dimensionless units are used. The effects of breaking integrability for the expectation values of the number operators are shown, with the initial state |60,0,0⟩. The configuration used has $U/J = 0.001$. **a** $\varepsilon/J = 0$; **b** $\varepsilon/J = 0.47$; **c** $\varepsilon/J = 1.0$; **d** $\varepsilon/J = 1.63$. It is apparent that increasing ε leads to greater suppression of tunneling into the drain. For **d** the expectation value of the number operator associated with the drain is negligible, so tunneling into the drain is considered to be switched-off

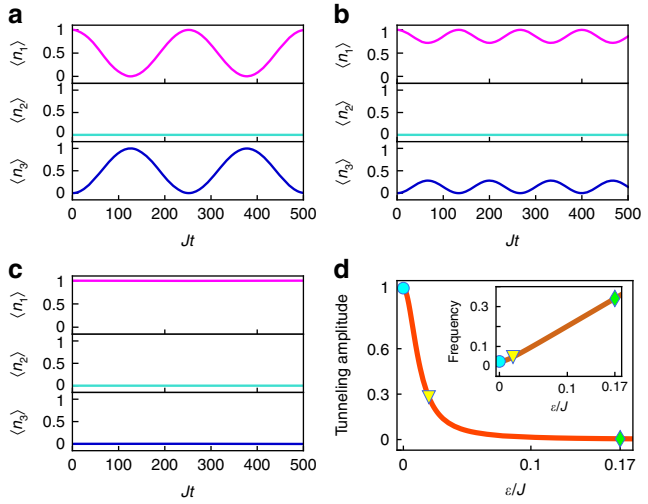

Fig. 5 Amplitude and frequency of oscillations. The configuration used has $N = 60$, $U/J = 0.17$, and initial state |60,0,0⟩. **a** Number operator expectation values for $\varepsilon/J = 0$: switched-on configuration, with maximum tunneling amplitude between the source and the drain. **b** Expectation values for $\varepsilon/J = 0.02$: ~30% of the maximal tunneling amplitude. **c** Expectation values for $\varepsilon/J = 0.17$: switched-off configuration. **d** Tunneling amplitude as a function of the external field ε/J. In the inset: tunneling frequency versus the external field ε/J. The markers in the curves correspond to the values of the amplitude of Fig. 5a (cyan circle), Fig. 5b (yellow triangle), and Fig. 5c (lime diamond)

approach harmonic oscillations with $\langle N_1\rangle + \langle N_3\rangle \simeq N$. The transition between the Rabi and Josephson regimes can be seen, qualitatively, in the passage from Fig. 3b and c. This change in behavior is in accord with the threshold point in Fig. 2.

In this latter regime, Fig. 3c and d, these dynamical features can be understood by observing that the integrable Hamiltonian possesses a hidden two-well algebraic structure, with an effective well given by the combined source and drain. As is known[1,2,31], the self-trapping regime is expected to occur in the two-well model in the Josephson regime. To be more precise, $\langle N_2\rangle/N < \tilde{\varepsilon}$ when $UN > J/(2\sqrt{\tilde{\varepsilon} - \tilde{\varepsilon}^2})$ if well 2 is initially empty. Thus, for $UN \gg J$, we find $\langle N_2\rangle/N \simeq 0$, and almost all bosons are distributed between the source and the drain if only a small fraction of bosons are initially in the gate.

On the other hand, it has been pointed out[19] that for isotropic tunneling the source and the drain can form an effective non-interacting two-well system, by second-order processes[32–34] through the gate, such that $\langle N_2\rangle \simeq 0$. For general tunneling, we find the remarkable result that the effective Hamiltonian is simply given by $H_{\rm eff} = -\lambda Q$, where Q is the conserved charge (3), and $\lambda^{-1} = 4U(N-1)$ (details are provided in Methods). This produces an effective tunneling coupling given by $J_{\rm eff} = \lambda J_1 J_3$, which decreases with increasing N, and therefore will only be observed in mesoscopic samples[19]. In view of the above observations, we formally identify the resonant tunneling regime of the system to be determined by $UN \gg J$, which contains the Josephson regime.

In Fig. 4, the time evolution of expectation values for number operators is displayed in a case of broken integrability. Increasing the value of ε suppresses the tunneling of particles into the drain, while increasing the time-average value of $\langle N_2\rangle$. For $\varepsilon/J = 1.63$ this suppression of tunneling into the drain is strong enough that its number expectation value is close to negligible, i.e. tunneling into the drain has been switched-off.

Control of resonant tunneling. In Fig. 3d, the dynamics is seen to be remarkably close to being harmonic over sufficiently short time scales, with the period monotonically increasing with interaction coupling U. This behavior supports the conclusion that the effective Hamiltonian for the resonant tunneling regime is simply related to the conserved charge Q. The frequency of oscillation in this regime is given by $\omega_{\rm J} = \lambda J^2$, with the amplitude also being U-dependent. When the initial state is |N,0,0⟩, the oscillations between the source and drain are coherent, with tunneling to the gate switched-off. On the other hand, if the initial state is |0,N,0⟩ the system will remain trapped in this initial state configuration, with tunneling from the gate switched-off.

Next, we maintain the system in the resonant tunneling regime $UN \gg J$ and study the non-integrable dynamics using the parameter ε to control the behavior of the source and drain subsystem. The approach here, following the study above, is to choose the initial state |N,0,0⟩ and investigate the ability to control the frequency and amplitude of the populations oscillating between the source and the drain.

In Fig. 5a–c, the interaction coupling is fixed as $U/J = 0.17$, and results are shown for the expectation values of the populations using three choices for ε. It is seen that the presence of the external field does not significantly influence the gate, in the sense that it does not affect the negligible average population $\langle N_2\rangle$. Figure 5d shows how the amplitude decays while increasing the external field, as well as the dependence of the frequency. The three points highlighted in the curves correspond to the values of the amplitude and frequency of Fig. 5a (cyan circle), Fig. 5b (yellow triangle), and Fig. 5c (lime diamond).

In this non-integrable regime the effective Hamiltonian is given by

$$H_{\rm eff} = -\lambda Q + \varepsilon(N_3 - N_1). \tag{5}$$

For short time scales the dynamics exhibits Josephson-like oscillation[28] with frequency

$$\omega_{\rm J} = \frac{2\lambda J_1 J_3}{\sqrt{\Delta n}}, \tag{6}$$

where $\Delta n = 1/(1+\gamma^2)$ is the amplitude and $\gamma = (\lambda(J_1^2 - J_3^2) - 2\varepsilon)/2\lambda J_1 J_3$ (see Methods for details). Increasing the external field reduces the oscillation amplitude Δn and the period between the source and the drain, until the amplitude of oscillation is completely suppressed, i.e., all tunneling is switched-off, demonstrating various levels of control, especially in the range $0 < \varepsilon < 0.2$. Through semiclassical analysis, one can obtain analytic expressions for the expectation values of the relative populations, $n_i \equiv N_i/N$ $(i = 1, 3)$, in the wells 1 and 3, given by $\langle n_1 \rangle = 1 - \langle n_3 \rangle$ and $\langle n_3 \rangle = \Delta n \sin^2(\omega_J t/2)$ (see details in Methods). In agreement with Chuang et al.[35], the maximum amplitude is obtained when the field is small.

Discussion

We have analyzed a model for boson tunneling in a triple-well system. This was conducted in both integrable and non-integrable settings through variation of coupling parameters. The model draws an analogy with a transistor through identification of the wells as the source, gate, and drain. Our primary objective was to investigate how this model could be implemented as an atomtronic switching device.

In the integrable setting, we identified the resonant tunneling regime between the source and drain, for which expectation values of particle numbers in the gate are negligible. Moreover, it was found that a conserved operator of the integrable system acts as an effective Hamiltonian, which predicts coherent oscillations. This is in agreement with observations from numerical calculations.

We then broke integrability through application of an external field to the source and the drain. It was shown in Fig. 4 that the applied field to the system, in Rabi regime, was able to switch-off tunneling to the drain. On the other hand, in the resonant tunneling regime, the field did not destroy the harmonic nature of the oscillations, but did influence the amplitude and frequency. Increasing the applied field allowed for tuning the system from the switched-on configuration through to switched-off (Fig. 5). Results from semiclassical analyses produced formulae for the amplitude and frequency, which proved to be remarkably accurate when compared to numerical calculations. This demonstrates the possibility to reliably control the harmonic dynamical behavior of the model in a particular regime. A surprising feature of this result is that the ability to control the system in a predictable manner arises through the breaking of integrability. Our results open possibilities for multi-level logic applications and consequently new avenues in the design of atomtronic devices.

It is important, finally, to comment on the limitations of a three-mode Hamiltonian in the description of cold atom systems in a triple-well potential. Contributions from higher energy levels of the single-particle spectrum cannot be ignored under certain coupling regimes. For example, the presence of the external field will ultimately lead to level crossings as the field strength is increased. In the case of the analogous double-well system, estimates for when this may occur have been formulated[36]. We have undertaken checks to confirm that it is indeed possible to avoid these undesired scenarios, within an experimentally feasible scenario. (See Supplementary Note 1, Supplementary Figure 1 for further details). However, it is also noteworthy that it is possible to include three-body, and higher, interaction terms as corrections[37] to compensate for when the three-mode approximation breaks down.

Methods

In this section, we provide the details concerning algebraic structures behind the model, and complementary semiclassical approximations, which were used to derive analytic expressions characterizing quantum control in the resonant tunneling regime. These expressions were found to give close agreement with results obtained by exact numerical diagonalization (see Supplementary Note 2, Supplementary Figures 2 and 3 for more details). We also discuss the feasibility of physical realization of the system.

Two-mode structure and the resonant tunneling regime. The integrable three-well model can be structured through two modes, as follows. From Eq. 2, we define $J = \sqrt{J_1^2 + J_3^2}$ and the operators $N_{1,3} = N_1 + N_3$, $a_{1,3} = J^{-1}(J_1 a_1 + J_3 a_3)$ and $a_{1,3}^\dagger = J^{-1}(J_1 a_1^\dagger + J_3 a_3^\dagger)$ satisfying the Heisenberg algebra

$$[N_{1,3}, a_{1,3}] = -a_{1,3}, [N_{1,3}, a_{1,3}^\dagger] = a_{1,3}^\dagger, [a_{1,3}, a_{1,3}^\dagger] = 1.$$

Then

$$H_0 = U(N_{1,3} - N_2)^2 + J(a_{1,3}^\dagger a_2 + a_2^\dagger a_{1,3}),$$

such that the modes of wells 1 and 3 are now represented by the single mode "1,3".

The two-well model exhibits a self-trapping regime, with onset in the vicinity of $\chi \equiv UN/J \simeq 1$[1,31]. This translates to a resonant tunneling regime for the triple-well model. Here we follow the approach of using semiclassical analysis[38], such that this regime may be clearly identified. Using the usual number-phase correspondence, that is, $a_2 = e^{i\theta_2}\sqrt{N_2}$, $a_{1,3} = e^{i\theta_{1,3}}\sqrt{N_{1,3}}$ and the conservation of boson number $N_{1,3} + N_2 = N$, we find

$$h = \frac{H_0}{N} = UN(1 - 2n_2)^2 + 2J\sqrt{(1 - n_2)n_2}\cos\phi,$$

where $n_2 = N_2/N$ and $\phi = \theta_{1,3} - \theta_2$. Consider the dynamics where the initial condition is $n_2 = 0$. At the initial time $t = 0$ the system has the energy $h = UN$. By energy conservation at all times, we obtain the expression

$$n_2 = \frac{1}{2} - \frac{\sqrt{\chi^2 - \cos^2\phi}}{2\chi}. \quad (7)$$

The conditions $\chi > 1$ and $|\cos\phi| = 1$ (maximum value) imply that $0 \le n_2 \le 0.5$. From Eq. (7), we conclude that when $\chi \gg |\cos\phi|$, $n_2 \to 0$, and the bosons are distributed between the wells labeled 1 and 3, producing the resonant tunneling regime.

Effective integrable Hamiltonian for resonant tunneling. In order to better understand the dynamics in the resonant tunneling regime, we first observe that the integrable Hamiltonian can be written, by using the conserved quantity N, as an effective Hamiltonian without on-site interaction (up to a global constant UN^2). Specifically $H_0 = H_I + V$, where the interaction term $H_I = -4UN_2(N_1 + N_3)$ has eigenstate and eigenvalues given by

$$H_I|\mathcal{N}_1, \mathcal{N}_2, \mathcal{N}_3\rangle = -4U\mathcal{N}_2(\mathcal{N}_1 + \mathcal{N}_3)|\mathcal{N}_1, \mathcal{N}_2, \mathcal{N}_3\rangle,$$

and the tunneling term $V = (J_1 a_1^\dagger + J_3 a_3^\dagger)a_2 + \text{h.c.}$ is treated as a perturbation. For the isotropic case $J_1 = J_3 = J/\sqrt{2}$[19], since $n_2 \simeq 0$ the interaction part is $H_I \simeq 0$ and the wells 1 and 3 form an effective non-interacting two-well system coupled through well 2 by a second-order process[19,32–34] with the effective Hamiltonian $H_{\text{eff}} = J_{\text{eff}}(a_1^\dagger a_3 + a_3^\dagger a_1)$. Recall that the transition rate from initial state $|s\rangle$ to final state $|k\rangle$ is expressed

$$W^{(i)} = 2\pi|\langle k|V^{(i)}|s\rangle|^2\delta(E_k - E_s), \qquad i = 1, 2,$$

where $V^{(1)} = V$ for first-order transition (Fermi's golden rule), δ is the delta function and

$$V^{(2)} = \sum_m \frac{V|m\rangle\langle m|V}{E_s - E_m}$$

for second-order transitions. Equating second-order transition of V with the first-order transition of H_{eff} for the states $|N,0,0\rangle$ and $|N-1,0,1\rangle$, it is found that

$$J_{\text{eff}} = \frac{J^2}{8U(N-1)}.$$

Observing that $J_3^2 N_1 + J_1^2 N_3$ is constant for isotropic tunneling in the regime $\chi \gg 1$, then it does not affect the dynamics if we consider the linear combination $J_{\text{eff}}(a_1^\dagger a_3 + a_3^\dagger a_1) + \lambda'(J_3^2 N_1 + J_1^2 N_3)$. By numerical inspection, we conclude that the effective Hamiltonian for general tunneling, which includes the anisotropic tunneling $J_1 \neq J_3$, is given by

$$H_{\text{eff}} = -\lambda Q,$$

where $Q = J_1^2 N_3 + J_3^2 N_1 - J_1 J_3(a_1 a_3^\dagger + a_1^\dagger a_3)$ is conserved and $\lambda^{-1} = 4U(N-1)$.

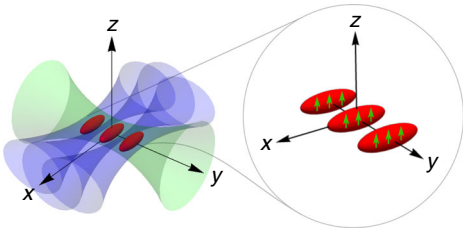

Fig. 6 Schematic representation of the trap geometry. Three parallel lasers (blue) are crossed by a transverse beam (green). The cigar-shapes, in red, represent a dipolar Bose–Einstein condensate trapped in a triple-well potential, and the green internal arrows depict the orientation of the dipoles

Effective non-integrable Hamiltonian and quantum control. For the non-integrable case, the effective Hamiltonian in the resonant tunneling regime $\chi \gg 1$ is given by $H_{\rm eff} = -\lambda Q + \varepsilon(N_3 - N_1)$. Returning to a semiclassical analysis it is found that, up to an irrelevant constant,

$$h = \frac{H_{\rm eff}}{N} = -\lambda J_1^2(1-n_1) - (\lambda J_3^2 + 2\varepsilon)n_1 + 2\lambda J_1 J_3 \sqrt{n_1(1-n_1)}\cos\varphi,$$

where $n_1 = N_1/N$ and $\varphi = \theta_1 - \theta_3$. For initial condition $n_1 = 1$ and $n_3 = 0$, we have $h = -\lambda J_3^2$, a constant. Applying energy conservation and the condition $\cos\varphi = \pm 1$, we find that the amplitude of oscillation Δn (Fig. 5d) is given by $\Delta n = 1/(1+\gamma^2)$, where $\gamma = [\lambda(J_1^2 - J_3^2) - 2\varepsilon]/2\lambda J_1 J_3$. Hamilton's equation gives

$$\dot{N}_1 = -\frac{\partial H_{\rm eff}}{\partial \theta_1} = 2\lambda J_1 J_3 \sqrt{N_1(N-N_1)}\sin\varphi, \Rightarrow \dot{n}_1 = 2\lambda J_1 J_3 \sqrt{n_1(1-n_1)}\sin\varphi.$$

Using the *Ansatz* $n_1 = 1 - \Delta n \sin^2(\eta t)$, we can easily verify that the above results provide analytic expressions for the expectation values

$$\langle n_1 \rangle = 1 - \Delta n \sin^2(\omega_J t/2), \quad \langle n_3 \rangle = \Delta n \sin^2(\omega_J t/2),$$

where ω_J is the frequency given by Eq. (6). Results for similar types of investigation have been presented in the case of pair-tunneling between two wells[34].

Physical realization. Here we discuss the feasibility of physical realization of the triple-well Hamiltonian (2), through use of Bose–Einstein condensates (BECs) of dipolar atoms.

Three parallel, tightly focused Gaussian beams, with waist of 1 μm and wavelength $\lambda = 1.064$ nm, separated by a distance $l = 1.8$ μm, form an optical triple-well potential aligned along the y-axis[19]. A transverse beam, with waist of 6 μm, provides xz-confinement. For such a setup, in the harmonic approximation the potential of each well $i = 1,2,3$ is symmetrically cylindrical and is given by

$$V_0(x,y,z) = \sum_{i=1}^{3}\left(\frac{1}{2}m\omega_x^2 x^2 + \frac{1}{2}m\omega_r^2((y-y_i)^2 + z^2)\right),$$

where $y_i = l, 0, -l$. The trap frequencies ω_x and ω_r can be controlled by the intensity of the laser beams. This configuration facilitates the formation of three cigar-shaped wells. We consider a system of bosons with dipole–dipole interactions to provide long-range interactions, and weakly repulsive contact interactions to promote condensate stability[39]. The dipoles are oriented along the z-direction (Fig. 6).

The transverse beam performs the function of the external field that controls the device. Its focus, when displaced along the y-axis by Δy, introduces the potential energy

$$V_1(y) = \frac{1}{2}m\omega_y^2 \Delta y(2y + \Delta y).$$

This generates a potential difference, resulting in the external field strength $\varepsilon = m\omega_y^2 \Delta y l$. The frequency of the transverse laser (ω_y) is much lower than the frequency of the parallel lasers (ω_r), so that displacement by Δy introduces a "tilting" of wells 1 and 3. These are the relevant wells in the resonant tunneling regime.

For the case of a dipolar BEC of ^{52}Cr[40], we numerically find that the integrability condition, with $\alpha \sim 5.8$, is achieved for $\omega_x \sim 2\pi \times 64$ Hz, $\omega_r \sim 2\pi \times 220$ Hz, where we assumed the Gaussian approximation for the ground state. The value of U obtained in units of J is $U/J \sim 7.5 \times 10^{-3}$, which means that the resonant tunneling regime can be achieved for $N \gg 130$ atoms. In principle, this condition can be satisfied experimentally[40]. As an example, for $N \sim 5000$ atoms, with $\omega_y \sim 2\pi \times 1.5$ Hz, translating the transverse laser by $\Delta y = 1.8$ μm we obtain $\varepsilon/h \sim 3.6 \times 10^{-2}$ Hz. It results in a tunneling amplitude $\Delta n \sim 0.25$, which means that 25% of the population of the source in the initial state $|N,0,0\rangle$ switch to the drain, and back, through harmonic tunneling. This example approaches the case of Fig. 5b.

Another strongly dipolar BEC which can be considered is ^{164}Dy[41]. In this case, we calculate $\alpha \sim 5.9$ for $\omega_x \sim 2\pi \times 22.7$ Hz, $\omega_r \sim 2\pi \times 67.3$ Hz with $U/J \sim 2.2 \times 10^{-2}$. For $N \sim 500$ atoms, with $\omega_y \sim 2\pi \times 0.76$ Hz, this yields $\varepsilon/h \sim 3.0 \times 10^{-2}$ Hz and $\Delta n \sim 0.23$.

In both cases above, the parameter choices are such that higher-order interaction terms, such as correlated hopping, are negligible[42].

An analysis of the effects of perturbations is provided in Supplementary Note 3: Fidelity dynamics, Supplementary Figures 4 and 5.

Data availability

All relevant data are available on reasonable request from the authors.

Received: 1 February 2018 Accepted: 8 November 2018
Published online: 07 December 2018

References

1. Milburn, G. J., Corney, J., Wright, E. M. & Walls, D. F. Quantum dynamics of an atomic Bose-Einstein condensate in a double-well potential. *Phys. Rev. A* **55**, 4318–4324 (1997).
2. Leggett, A. J. Bose-Einstein condensation in the alkali gases: some fundamental concepts. *Rev. Mod. Phys.* **73**, 307–356 (2001).
3. Albiez, M., Gati, R., Fölling, J., Hunsmann, S., Cristiani, M. & Oberthaler, M. K. Direct observation of tunneling and nonlinear self-trapping in a single bosonic Josephson junction. *Phys. Rev. Lett.* **95**, 010402 (2005).
4. Levy, S., Lahoud, E., Shomroni, I. & Steinhauer, J. The a.c. and d.c. Josephson effects in a Bose-Einstein condensate. *Nature* **449**, 579–583 (2007).
5. Cao, L., Brouzos, I., Zöllner, S. & Schmelcher, P. Interaction-driven interband tunneling of bosons in the triple well. *New J. Phys.* **13**, 033032 (2011).
6. Cao, L., Brouzos, I., Chatterjee, B. & Schmelcher, P. The impact of spatial correlation on the tunneling dynamics of few-boson mixtures in a combined triple well and harmonic trap. *New J. Phys.* **14**, 093011 (2012).
7. Benseny, A., Gillet, J. & Busch, T. Spatial adiabatic passage via interaction-induced band separation. *Phys. Rev. A* **93**, 033629 (2016).
8. Stickney, J. A., Anderson, D. Z. & Zozulya, A. A. Transistorlike behavior of a Bose-Einstein condensate in a triple-well potential. *Phys. Rev. A* **75**, 013608 (2007).
9. Seaman, B. T., Krämer, M., Anderson, D. Z. & Holland, M. J. Atomtronics: ultracold-atom analogs of electronic devices. *Phys. Rev. A* **75**, 023615 (2007).
10. Olsen, M. K. & Bradley, A. S. Quantum ultracold atomtronics. *Phys. Rev. A* **91**, 043635 (2015).
11. Dumke, R. et al. Roadmap on quantum optical systems. *J. Opt.* **18**, 093001 (2016).
12. Zhang, Z., Dunjko, V. & Olshanii, M. Atom transistor from the point of view of nonequilibrium dynamics. *New J. Phys.* **17**, 125008 (2015).
13. Marchukov, O. V., Volosniev, A. G., Valiente, M., Petrosyan, D. & Zinner, N. T. Quantum spin transistor with a Heisenberg spin chain. *Nat. Commun.* **7**, 13070 (2016).
14. Nemoto, K., Holmes, C. A., Milburn, G. J. & Munro, W. J. Quantum dynamics of three coupled atomic Bose-Einstein condensates. *Phys. Rev. A* **63**, 013604 (2000).
15. Buonsante, P., Franzosi, R. & Penna, V. Control of unstable macroscopic oscillations in the dynamics of three coupled Bose condensates. *J. Phys. A Math. Theor.* **42**, 285307 (2009).
16. Guo, Q., Chen, X. & Wu, B. Tunneling dynamics and band structures of three weakly coupled Bose-Einstein condensates. *Opt. Express* **22**, 19219–19234 (2014).
17. Olsen, M. K. Quantum dynamics and entanglement in coherent transport of atomic population. *J. Phys. B At. Mol. Opt. Phys.* **47**, 095301 (2014).
18. Gallemí, A., Guilleumas, M., Martorell, J., Mayol, R., Polls, A. & Juliá-Díaz, B. Fragmented condensation in Bose–Hubbard trimers with tunable tunnelling. *New J. Phys.* **17**, 073014 (2015).
19. Lahaye, T., Pfau, T. & Santos, L. Mesoscopic ensembles of polar bosons in triple-well potentials. *Phys. Rev. Lett.* **104**, 170404 (2010).
20. Ymai, L., Tonel, A., Foerster, A. & Links, J. Quantum integrable multi-well tunneling models. *J. Phys. A* **50**, 264001 (2017).
21. Caux, J.-S. & Mossel, J. Remarks on the notion of quantum integrability. *J. Stat. Mech.* **2011**, P02023 (2011).
22. Larson, J. Integrability versus quantum thermalization. *J. Phys. B At. Mol. Opt. Phys.* **46**, 224016 (2013).

23. D'Alessio, L., Kafri, Y., Polkovnikov, A. & Rigol, M. From quantum chaos and eigenstate thermalization to statistical mechanics and thermodynamics. *Adv. Phys.* **65**, 239–362 (2016).
24. Berry, M. V. & Tabor, M. Level clustering in the regular spectrum. *Proc. R. Soc. Lond. A* **356**, 375–394 (1977).
25. Wigner, E. P. On the statistical distribution of the widths and spacings of nuclear resonance levels. *Math. Proc. Camb. Philos. Soc.* **47**, 790–798 (1951).
26. Dyson, F. J. Statistical theory of the energy levels of complex systems II. *J. Math. Phys.* **3**, 157–165 (1962).
27. Poilblanc, D., Ziman, T., Bellissard, J., Mila, F. & Montambaux, G. Poisson vs. GOE statistics in integrable and non-integrable quantum Hamiltonians. *Europhys. Lett.* **22**, 537–542 (1993).
28. Kinoshita, T., Wenger, T. & Weiss, D. S. A quantum Newton's cradle. *Nature* **440**, 900–903 (2006).
29. Santos, L. F. & Rigol, M. Onset of quantum chaos in one-dimensional bosonic and fermionic systems and its relation to thermalization. *Phys. Rev. E* **81**, 036206 (2010).
30. Peter, D., Pawlowski, K., Pfau, T. & Rzażewski, K. Mean-field description of dipolar bosons in triple-well potentials. *J. Phys. B At. Mol. Opt. Phys.* **45**, 225302 (2012).
31. Tonel, A. P., Links, J. & Foerster, A. Quantum dynamics of a model for two Josephson-coupled Bose–Einstein condensates. *J. Phys. A* **38**, 1235–1245 (2005).
32. Duan, L.-M., Demler, E. & Lukin, M. D. Controlling spin exchange interactions of ultracold atoms in optical lattices. *Phys. Rev. Lett.* **91**, 090402 (2003).
33. Kuklov, A. B. & Svistunov, B. V. Counterflow superfluidity of two-species ultracold atoms in a commensurate optical lattice. *Phys. Rev. Lett.* **90**, 100401 (2003).
34. Fölling, S., Trotzky, S., Cheinet, P., Feld, M., Saers, R., Widera, A., Müller, T. & Bloch, I. Direct observation of second-order atom tunnelling. *Nature* **448**, 1029–1032 (2007).
35. Chuang, H. C., Salim, E. A., Vuletic, V., Anderson, D. Z. & Bright, V. M. Multi-layer atom chips for atom tunneling experiments near the chip surface. *Sens. Actuators A Phys.* **165**, 101–106 (2011).
36. Dounas-Frazer, D. R., Hermundstad, A. M. & Carr, L. D. Ultracold bosons in a tilted multilevel double-well potential. *Phys. Rev. Lett.* **99**, 200402 (2007).
37. Dobrzyniecki, J., Li, X., Nielsen, A. E. B. & Sowiński, T. Effective three-body interactions for bosons in a double-well confinement. *Phys. Rev. A* **97**, 013609 (2018).
38. Rubeni, D., Isaac, P. S., Links, J. & Foerster, A. Two-site Bose-Hubbard model with nonlinear tunneling: classical and quantum analysis. *Phys. Rev. A* **95**, 043607 (2017).
39. Koch, T., Lahaye, T., Metz, J., Fröhlich, B., Griesmaier, A. & Pfau, T. Stabilization of a purely dipolar quantum gas against collapse. *Nat. Phys.* **4**, 218–222 (2008).
40. Lahaye, T., Menotti, C., Santos, L., Lewenstein, M. & Pfau, T. The physics of dipolar bosonic quantum gases. *Rep. Prog. Phys.* **72**, 126401 (2009).
41. Barbut, I. F., Kadau, H., Schimitt, M., Wenzel, M. & Pfau, T. Observation of quantum droplets in a strongly dipolar bose gas. *Phys. Rev. Lett.* **116**, 215301 (2016).
42. Mazzarella, G., Giampaolo, S. M. & Illuminati, F. Extended Bose Hubbard model of interacting bosonic atoms in optical lattices: from superfluidity to density waves. *Phys. Rev. A* **73**, 013625 (2006).

Acknowledgements

K.W.W. and A.F. were supported by CNPq (Conselho Nacional de Desenvolvimento Científico e Tecnológico), Brazil. J.L. and A.F. were supported by the Australian Research Council through Discovery Project DP150101294. We thank Henri Boudinov, Ricardo R. B. Correia, Matt Davis, and Artem Volosniev for helpful discussions.

Author contributions

All authors contributed to the conceptualization of the project, and actively engaged in the writing of the manuscript. K.W.W., L.H.Y., and A.P.T. implemented the theoretical analyses of the model, detailed the experimental feasibility, and processed the numerical computations. J.L. and A.F. designed the research framework, and directed the program of activities.

Additional information

Supplementary Information accompanies this paper at https://doi.org/10.1038/s42005-018-0089-1.

Competing interests: The authors declare no competing interests.

Reprints and permission information is available online at http://npg.nature.com/reprintsandpermissions/

Publisher's note: Springer Nature remains neutral with regard to jurisdictional claims in published maps and institutional affiliations.